

# Hydrogen model atmospheres for white dwarf stars

R. D. Rohrmann<sup>★</sup>

*Observatorio Astronómico, Universidad Nacional de Córdoba, Laprida 854, (5000) Córdoba, Argentina*

January 10

## ABSTRACT

We present a detailed calculation of model atmospheres for DA white dwarfs. Our atmosphere code solves the atmosphere structure in local thermodynamic equilibrium with a standard partial linearization technique, which takes into account the energy transfer by radiation and convection. This code incorporates recent improved and extended data base of collision induced absorption by molecular hydrogen. We analyse the thermodynamic structure and emergent flux of atmospheres in a range  $2500 \leq T_{eff} \leq 60000$  K and  $6.5 \leq \log g \leq 9.0$ . Bolometric correction and colour indices are provided for a subsample of the model grid. Comparison of the colours is made with published observational material and results of other recent model calculations.

Motivated by the increasing interest on helium core white dwarfs, we analyse the photometric characteristics of these stars during their cooling, using evolutionary models recently available. Effective temperatures, surface gravities, masses and ages have been determined for some helium core white dwarf candidates, and their possible binary nature is briefly discussed.

**Key words:** stars: atmospheres - white dwarfs - stars: fundamental parameters

## 1 INTRODUCTION

White dwarf (WD) stars represent the most common end-product of the stellar evolution. On average, WDs have a mass of  $0.6M_{\odot}$ , a central density of  $10^6$  gr  $\text{cm}^{-3}$  and a core composed of carbon and oxygen resulting from helium burning during the preceding phases of the evolution (D’Antona & Mazzitelli 1990). Due to the high degree of electron degeneracy in the interior of WDs, the outer nondegenerate layers, and specially their atmospheres, control the loss of energy into outer space and therefore, the cooling of these objects. From a technical view point, detailed atmosphere models provide an adequate surface boundary condition for the computation of evolutionary stellar models. Besides, the atmosphere models are necessary to determine the emergent flux from the star, which is required to interpret the luminosities and colours of observed WDs.

Current interest in WDs is motivated by two reasons. These stars are candidates for the Galactic dark matter and can also be used to estimate the age of the star system they belong to. The recent detection of gravitational microlensing events in the direction of the Magellanic Clouds (Alcock et al. 1997, Alcock et al. 1999, Renault et al. 1997) suggests that very low mass stars, WDs among others, might constitute a significant fraction of the mass of the Galactic halo.

The luminosity function necessary to study this interpretation requires the calculation of cooling tracks using accurate atmosphere models.

The spectral evolution of a WD during its cooling can be used to calculate the age of the star. The first detailed calculation of WD evolution was performed by Iben & Tutukov (1984), for the cooling of a carbon-oxygen WD from the planetary nucleus stage through the stage of complete internal crystallization. Recent works (Hansen 1999; Chabrier 1999) show that the time scales involved, particularly in an advanced stage of the cooling process, depend strongly on the atmosphere composition (among other factors such as the stellar mass), which through the opacity regulates the energy loss from the stellar interior. Thus, for instance, the strong opacity from hydrogen molecules causes a slow cooling of the WDs with hydrogen-rich atmosphere, resulting these objects potentially observable for times comparable to the Hubble time (Richer et al. 2000). The technique based on the observation of a low-luminosity cutoff has been applied to estimate the age of the local Galactic disk (Winget et al. 1987; Wood 1992) and the age of clusters (von Hippel, Gilmore & Jones 1995; von Hippel & Gilmore 2000).

The majority of WDs have pure hydrogen atmospheres due to gravitational settling, which is efficient at removing helium and heavier elements from atmosphere toward inner layers (Fontaine & Michaud 1979; Muchmore 1984; Iben & MacDonald 1985; Althaus & Benvenuto 2000). Convective mixing could lead to a helium-rich atmosphere in cool WD

<sup>★</sup> Fellow of the Consejo Nacional de Investigaciones Científicas y Técnicas (CONICET), Argentina. Email: rohr@oac.uncor.edu

when the mass of the superficial hydrogen layer is small enough (Koester 1976; Vauclair & Reisse 1977; D’Antona & Mazzitelli 1979). In particular, Bergeron, Ruiz & Leggett (1997) have reported evidence for convective mixing in cool WD atmospheres. However, hydrogen-rich atmospheres are observationally most abundant than those of helium or other with metals, in part due to the long cooling times. Furthermore, these atmospheres present a structure which is insensitive to small admixtures of helium (Hansen 1999).

In this context, recent model atmosphere calculations (Hansen 1998, 1999; Saumon & Jacobson 1999) suggest that WDs of very low luminosity, and therefore very old, become bluer and not redder as they age (and their effective temperature decreases), resulting their detection easier. This being the case, an important number of these objects should be observed with the new generation of telescopes.

Another important question of current interest is the evolution of WDs with very low mass having helium cores (He WD). Such stars, due to the low stellar mass, would be formed from some binary systems. Indeed, numerous binary configurations of this type have been observed lately (Marsh 1995; Moran, Marsh & Bragaglia 1997; Edmonds et al. 1999). In particular, low mass WDs have been detected in binary systems composed of a WD star and a pulsar. A particularly interesting binary system with these characteristics is the millisecond pulsar J1012+5307 and its WD companion, because it is possible to determine the properties of the pulsar from the analysis of the WD (Van Kerwijk, Bergeron & Kulkarni 1996). The study of these binaries would allow us to determine an upper limit to the neutron-star mass (and in this way, to constrain the still uncertain properties of the equation of state of the cool nuclear matter) and on its age (with implications for the evolution of its magnetic field). Obviously, to obtain accurate results from the study of these systems it is necessary to have suitable evolution models and, in particular, detailed model atmospheres for WDs.

The primary aim of this paper is to present results of model calculations from an independent atmosphere code. This will be applied to determine accurate cooling tracks of WDs, by providing appropriate outer boundary conditions to evolution models. Our model atmospheres with pure hydrogen compositions cover extensive ranges of effective temperature ( $2500 \leq T_{eff} \leq 60000$  K) and surface gravity ( $6.5 \leq \log g \leq 9.0$ ). Although several sets of models available in the literature (cf. Bergeron, Ruiz & Leggett 1997; Saumon & Jacobson 1999; Hansen 1999; Chabrier 1999) have already investigated different parts of this ( $T_{eff}, g$ ) region, we offer here an overall analysis. We have considered it important to extend the study to the very low gravities ( $\log g = 6.5$ ) which are found in early stages of the WD formation, and also in the cool stages of He WDs with very low mass, which have received little or no attention so far. In particular, we have also computed model atmospheres following the cooling tracks of He WDs with hydrogen envelopes and several masses.

The results presented here are based on ideal equations of state. The incorporation of density effects in our code using the occupation probability formalism of Hummer & Mihalas (1988) is in progress. However, nonideal effects can be neglected for hydrogen WD models with  $T_{eff} \geq 4000$  K (Bergeron, Saumon & Wesemael 1995a). They increase for

lower  $T_{eff}$  and are significant for  $T_{eff} \leq 2500$  K (Saumon & Jacobson 1999).

In Section 2 we derive explicit analytical expressions for the thermodynamic quantities required in the calculations. The method used for the model atmosphere computations is presented in Section 3, together with the opacities and convective theory adopted. In Section 4 we display the atmosphere structure of WDs obtained from our code. Comparisons with observations and other recent model results, through the analysis of colour diagrams, are also presented there. Our conclusions are given in Section 5.

## 2 THERMODYNAMIC QUANTITIES

The computation of convective flux of energy requires some properties of the gas such as the adiabatic gradient and the specific heat. To determine them, we consider a mixture of  $H_2$ , H,  $H^+$ ,  $e^-$ , and radiation occupying a volume  $V$ , in thermodynamic equilibrium at temperature  $T$ . In the present calculations, species with low abundances can be ignored (Saumon & Chabrier 1992).

Let  $N$  be the number of hydrogen nuclei or protons. Then, the number conservation and charge neutrality constraints demand that the particle density is

$$\frac{xN}{V}, \quad (1)$$

with

$$x = 1 + x_1 - x_2, \quad (2)$$

where  $x_1 = n_{H^+}/n$  and  $x_2 = n_{H_2}/n$  (with  $n = N/V$ ) are the number concentration of  $H^+$  and  $H_2$ . We use the ideal state equation to express the gas pressure. The total pressure, including the radiation contribution, is then

$$P = \frac{xNkT}{V} + \frac{1}{3}aT^4. \quad (3)$$

We adopt a simple approach for the total energy in the system

$$U = \frac{3}{2}xNkT + \left[ x_1\chi_1 + \left( \frac{1}{2} - x_2 \right) \chi_2 \right] N + \left[ kT + kT_v \left( \frac{1}{2} + \frac{1}{e^\theta - 1} \right) \right] x_2N + aT^4V, \quad (4)$$

where  $\theta = T_v/T$ . The first term on the right-hand side is the translational energy, which assumes the particles to behave as classical point particles. The second term gives the potential energy of the hydrogen nuclei, which increases with the dissociation of  $H_2$  molecules and the ionization of H atoms according to the corresponding binding energies  $\chi_1$  and  $\chi_2$ . For simplicity, we ignore in this term the excited states of these species. The zero point of the energy scale is taken to be the ground state of  $H_2$ . The third term represents the rotation-vibration energy of  $H_2$ , where we use a vibration temperature  $T_v = 6100$  K. Finally, the last term takes into account the energy in the radiation field.

Expressions for the adiabatic gradient  $\nabla_A = \partial \ln T / \partial \ln P|_S$ , and heat capacity at constant pressure  $C_P = \partial U / \partial T|_P + P \partial V / \partial T|_P$ , can be obtained from differentiation of Equations (3) and (4). We have followed a similar procedure to that of Krishna-Swamy (1961; see also Mihalas 1965) and, therefore, we only show here the results obtained

including molecular species in the gas mixture. The expression for the adiabatic gradient is

$$\nabla_A = \frac{a_1}{a_2}, \quad (5)$$

with

$$a_1 = 1 + 4\gamma - b_1 \left. \frac{\partial x_1}{\partial \ln P_g} \right|_T + b_2 \left. \frac{\partial x_2}{\partial \ln P_g} \right|_T \quad (6)$$

and

$$a_2 = \frac{5}{2} + 16\gamma + \left[ 1 + \frac{\theta^2 e^{-\theta}}{(1 - e^{-\theta})^2} \right] \frac{x_2}{x} + b_1 \left. \frac{\partial x_1}{\partial \ln T} \right|_{P_g} - b_2 \left. \frac{\partial x_2}{\partial \ln T} \right|_{P_g}, \quad (7)$$

where

$$b_1 = \left( \frac{5}{2} + \frac{\chi_1}{kT} + 4\gamma \right) \frac{1}{x}, \quad (8)$$

$$b_2 = \left\{ \frac{5}{2} + \frac{\chi_2}{kT} + 4\gamma - \left[ 1 + \theta \left( \frac{1}{2} + \frac{e^{-\theta}}{1 - e^{-\theta}} \right) \right] \right\} \frac{1}{x}. \quad (9)$$

For the heat capacity we obtain

$$\begin{aligned} \frac{C_P}{kN} = & \left[ \frac{3}{2} + 12\gamma + (1 + 4\gamma)^2 \right] x \\ & + \left[ 1 + \frac{\theta^2 e^{-\theta}}{(1 - e^{-\theta})^2} \right] x_2 + \left( \frac{3}{2} + \frac{\chi_1}{kT} \right) \left. \frac{\partial x_1}{\partial \ln T} \right|_P \\ - & \left\{ \frac{3}{2} + \frac{\chi_2}{kT} - \left[ 1 + \theta \left( \frac{1}{2} + \frac{e^{-\theta}}{1 - e^{-\theta}} \right) \right] \right\} \left. \frac{\partial x_2}{\partial \ln T} \right|_P. \end{aligned} \quad (10)$$

The partial derivatives of the concentrations  $x_1$  and  $x_2$ , have been calculated considering that, except in the regime of pressure dissociation,  $\text{H}^+$  and  $\text{H}_2$  do not have simultaneously high abundances. Then, using Saha equations for the first and third reactions in Table 1, result

$$\left. \frac{\partial x_1}{\partial \ln P_g} \right|_T = -\frac{x_1}{2} (1 - x_1^2), \quad (11)$$

$$\left. \frac{\partial x_1}{\partial \ln T} \right|_{P_g} = \frac{x_1}{2} (1 - x_1^2) \left( \frac{5}{2} + \frac{\chi_1}{kT} \right), \quad (12)$$

$$\left. \frac{\partial x_1}{\partial \ln T} \right|_P = \frac{x_1}{2} (1 - x_1^2) \left( \frac{5}{2} + \frac{\chi_1}{kT} + 4\gamma \right), \quad (13)$$

$$\left. \frac{\partial x_2}{\partial \ln P_g} \right|_T = \left( \frac{1}{x_2} + \frac{4}{1 - 2x_2} - \frac{1}{1 - x_2} \right)^{-1}, \quad (14)$$

$$\left. \frac{\partial x_2}{\partial \ln T} \right|_{P_g} = - \left( \frac{5}{2} + \frac{\chi_2}{kT} \right) \left. \frac{\partial x_2}{\partial \ln P_g} \right|_T, \quad (15)$$

$$\left. \frac{\partial x_2}{\partial \ln T} \right|_P = - \left( \frac{5}{2} + \frac{\chi_2}{kT} + 4\gamma \right) \left. \frac{\partial x_2}{\partial \ln P_g} \right|_T, \quad (16)$$

where the dependence of the partition functions with the temperature and pressure has been neglected.

Since the adiabatic temperature gradient forms the basis of the Schwarzschild criterion for convective instability, this gradient plays a central role in the computation of atmosphere models. Therefore, we check our expression (5-7) by comparing with results from the equation of state (EOS)

for hydrogen developed by Saumon & Chabrier (summarized in Saumon, Chabrier & Van Horn 1995, SCVH). This EOS, considered the best available at present for hydrogen, is based on the free-energy minimization technique (for details, see Graboske, Harwood & Rogers 1969; Fontaine, Graboske & Van Horn 1977; Hummer & Mihalas 1988) and includes a sophisticated treatment of nonideal effects.

Comparisons between values for the adiabatic gradient obtained from SCVH and our EOS are shown in Fig. 1. The curves correspond to models of WD atmosphere with  $T_{eff} = 2500, 4000, 6000$  and  $10000$  K, and  $\log g = 8$ . Both present and SCVH calculations agree quite well except for high pressures of the model  $T_{eff} = 2500$  K, where non-ideal effects can be present. For the hottest two models, discrepancies at low pressure occur beyond the regime where SCVH EOS can be applied ( $4 < \log P(\text{dyn cm}^{-2}) < 19$ ). In particular, the upper layers of the  $T_{eff} = 6000$  K atmosphere are dominated by atomic hydrogen (see Section 4.1), and a tendency to a value 0.4 for the temperature gradient (corresponding to an ideal monoatomic gas) is reproduced by our calculations. A partial molecular formation (up to  $n_{\text{H}_2}/n = 0.12$ ) takes place as one proceeds inward in this atmosphere, yielding a dramatic drop in the value of  $\nabla_A$ .

Other familiar features can be identified in this figure. For instance,  $T_{eff} = 2500$  K model represents an atmosphere formed mainly by  $\text{H}_2$ . At low temperatures present in its superficial layers, the  $\text{H}_2$  vibrational modes remain frozen and then, the adiabatic gradient takes a value close to  $2/7 = 0.286$ , i.e. that due to a fluid of rigid rotating molecules with two degrees of rotational freedom and three degrees of translational freedom. The adiabatic gradient decreases toward deep layers where the molecular gas is partially dissociated.

The low values reached by  $\nabla_A$  in the  $T_{eff} = 4000$  K model are due to a marked sensitivity of the molecular abundance to changes in temperature and pressure. While the behaviour of  $\nabla_A$  in the hottest model ( $T_{eff} = 10000$  K) is produced by different ionization degree at different depth.

In conclusion, the relative simplicity of our EOS allows us to obtain the analytic expressions for the heat capacity and the adiabatic gradient necessary to compute atmosphere models. This has the advantage of avoiding potential errors due to numerical inaccuracies that can be present in a sophisticated EOS, which requires interpolation from tables and numerical evaluation of derivatives.

### 3 MODEL ATMOSPHERE

Cooling of WDs is a very slow process so that the atmosphere structure responds to quasi-static boundary conditions. Furthermore, the region where the emergent radiation is formed has a thickness much less than the stellar radius. These properties allow us to choose a static model atmosphere with the approximation of plane-parallel layers and constant surface gravity throughout the atmosphere.

On the other hand, because the gas densities are very high in the layers where the emergent radiation is formed, local thermodynamic equilibrium (LTE) is a good approximation for the matter state and we adopt that.

We take the atmosphere gas to be composed of  $\text{H}$ ,  $\text{H}_2$ ,  $\text{e}^-$ ,  $\text{H}^-$ ,  $\text{H}^+$ ,  $\text{H}_2^+$  and  $\text{H}_3^+$ . The main constituents are  $\text{H}_2$ ,

**Table 1.** Reactions considered at the chemical equilibrium.

Reaction	ionization/dissociation energy (eV)
$\text{H} \rightarrow \text{H}^+ + \text{e}^-$	13.598
$\text{H}^- \rightarrow \text{H} + \text{e}^-$	0.755
$\text{H}_2 \rightarrow 2\text{H}$	4.478
$\text{H}_2^+ \rightarrow \text{H} + \text{H}^+$	2.651
$\text{H}_3^+ \rightarrow \text{H}_2 + \text{H}^+$	4.354

H,  $\text{H}^+$  and  $\text{e}^-$ , depending on the physical conditions. The other species are usually present as traces, but they can play an important role in the absorption and emission of radiation. In fact, the  $\text{H}^-$  ion can be a dominant source of opacity in cool atmospheres, whereas  $\text{H}_2^+$  and  $\text{H}_3^+$  are important because their presence affects the concentration of  $\text{H}^-$  and  $\text{e}^-$ .

To determine the equilibrium concentrations we consider the reactions given in Table 1. The values of energy are those compiled by Lenzuni & Saumon (1992). We use the partition functions calculated by Irwin (1981) for H and  $\text{H}_2$ , by Sauval & Tatum (1984) for  $\text{H}_2^+$ , and Neale & Tenynson (1995) for  $\text{H}_3^+$ . We have checked our chemical equilibrium against results from an independent code (Saumon 1999; based on an equation of ideal state, except in a sharp cutoff in the H partition function depending on the distance to the nearest neighbor). Though some differences (at most 12%) appear between both calculations (mainly due to different ways of computing the  $\text{H}_2$  partition function), the agreement is satisfactory in general.

### 3.1 Opacities

We have consider the most important opacity sources in a hydrogen atmosphere. Bound-free and free-free absorption coefficients of H have been taken from Mihalas (1978), with Gaunt factors from Menzel & Pekeris (1935). Isotropic Thomson scattering is assumed for the opacity of free electrons. We adopted absorption coefficients of the negative hydrogen ion according to John (1988) for bound-free transitions, and analytic fits by Gray (1992) based on Bell & Berrington (1987) results for free-free transitions.

Collisions between  $\text{H}_2$  molecules yield collision-induced absorption (CIA), consisting of rototranslational and rovibrational bands with peaks located in far-red and infrared spectral regions. We use  $\text{H}_2$ - $\text{H}_2$  CIA cross sections calculated by Borysow and coworkers, including the most recent results (Borysow, Jorgensen & Zheng 1997). For increasingly large densities, absorption from collisions involving more than two  $\text{H}_2$  molecules becomes important. Three-body collisions are no longer negligible for densities  $\rho > 0.02 \text{ g cm}^{-3}$  and they dominate the opacity above  $\rho > 0.2 \text{ g cm}^{-3}$  (Lenzuni & Saumon 1992). Ignoring terms of higher order, the total frequency-integrated CIA coefficient can be expressed as (Lenzuni, Chernoff & Salpeter 1991)

$$k = k_2\rho^2 + k_3\rho^3, \quad (17)$$

where  $k_2$  and  $k_3$  account for absorption by binary and ternary collisions. We assume the ratio  $k_3/k_2 = 0.05/\rho$  measured experimentally by Hare & Welsh (1958).

Finally, cross section of Rayleigh scattering from molecular hydrogen is taken from Dalgarno & Willians (1966). We

also consider other opacity sources such as Rayleigh scattering from H, bound-free and free-free absorption of  $\text{H}_2^+$ , and free-free opacity of  $\text{H}_2^-$ . For all of them, we use coefficient expressions from Kurucz (1970).

### 3.2 Convective Transport

Energy transport by convection is treated within the mixing-length theory (e.g., Cox & Giuli 1968; Mihalas 1978) in most model atmosphere calculations of WDs. Although this phenomenological formalism involves free parameters, Bergeron, Wesemael & Fontaine (1992) have found that model results with  $T_{eff}$  below  $\approx 8000 \text{ K}$  are insensitive to the assumed parameterization. In addition, they found that the predicted emergent fluxes show dependence on the efficiency of convection in the range  $T_{eff} \approx 8000\text{-}15000 \text{ K}$ . However, it is difficult to decide which is the most appropriate parameterization for WDs. Preliminary analyses of the effects of convective efficiency on atmospheric parameters of ZZ Ceti<sup>†</sup> and other lukewarm DA stars, suggest that ML1 and ML3 parameterizations (following the nomenclature of Fontaine, Villeneuve & Wilson 1981) could be inadequate (Wesemael et al. 1991, Bergeron et al. 1992). In this context, the ML2 version of the mixing-length theory has been considered a viable alternative. The results presented here use this version of convection.

### 3.3 Numerical Method

The model atmosphere may be calculated using an iteration procedure over linearized structure equations in terms of perturbations of the temperature and density (or pressure). However, we adopt a linearization method for the temperature alone (Gustafsson 1971), the density and pressure structure being obtained from a given temperature distribution by integration of the hydrostatic equilibrium equation. This procedure yields similar results to a complete linearization method, but has a much shorter computing time (Saumon et al. 1994; SBLHB). Additional economy of execution time is obtained from formulating the radiative transfer in terms of moment equations, with closure using variable Eddington factors (Auer & Mihalas 1970).

To calculate a model atmosphere, the equations of radiative transfer and constant flux condition are linearized as functions of the temperature. The equations are discretized and organized following the Rybicki scheme (for details see Gustafsson 1971 and Gustafsson & Nissen 1972). The calculation of a model starts with a given temperature distribution from which the hydrostatic equilibrium equation is integrated, and the opacities and thermodynamic quantities derived. Then, transfer and energy constrain equations are solved and we obtain a temperature correction. The whole process is iterated to convergence. The Eddington factors are evaluated in each step from a Feautrier solution of the radiative transfer, using known values of the source function.

<sup>†</sup> WDs of DA class (i.e. with Balmer lines and no He I or metals present, and therefore, having H-rich atmospheres) showing non-radial pulsations.

### 3.4 Model convergence properties

We remark on some points about the performance of the calculations. Although the correction procedure adopted here has proved effective and stable, certainly it is not as stable as when the energy transfer is purely radiative. Numerical difficulties can appear to solve the coupled equations of transfer and conservation energy when both convective and radiative modes are present (Gustafsson 1971; Grenfell 1974; Koester 1980; Bergeron et al. 1991; SBLHB). These difficulties are not exclusive to partial or complete linearization methods, since they have also been reported by Mihalas (1965) using a modification of the temperature-correction method proposed by Avrett and Krook (1963).

We found that numerical instability can occur mainly in atmospheres of WDs with low  $T_{eff}$  and high gravity. In these models, the convection becomes extremely efficient and, therefore, the temperature gradient is nearly adiabatic ( $\nabla - \nabla_A < 10^{-3}$  in convective deep layers). Then, the temperature correction oscillates yielding a large convective flux in one iteration, and zero convection in that following for the same layer, according to the Schwarzschild instability criterion. Among the different ways that have been proposed to stabilize the iterations (see above references), we found convenient a similar method to the one suggested by Koester (1980). This consists of setting  $F_c = F - F_{rad}$  instead of  $F_c = 0$  when  $\nabla < \nabla_A$  for a layer which would be convective in the converged model.

On the other hand, a good initial temperature distribution decreases the number of iterations necessary and increases the range of convergence of the model in the ( $T_{eff}$ ,  $\log g$ ) plane. For purely radiative models, one can start with an approximate solution of the gray atmosphere problem, e.g. the Eddington distribution (Mihalas 1978). However, when the convection is present, this class of distributions usually leads to an enormous convective flux which may have destabilizing consequences on the temperature correction method. A more suitable starting model is obtained when in the convective zone where  $F_c > F$ , the temperature gradient is changed and forced to yield  $F_c = F$  (Nordlund 1974). This procedure yields a suitable initial temperature stratification in convective models, from which to apply the rigorous temperature correction scheme.

Finally, as in the report of SBLHB, we found that a discontinuity develops in the temperature distribution of converged models with  $T_{eff} \approx 4400$ -5500 K at  $\log g \gtrsim 7.5$ , extending to lower effective temperatures when the gravity decrease. Such as discussed further by Bergeron et al. (1995a), this effect is due to competition between opacities of  $H_2$  molecule and hydrogen negative ion. This convergence problem can be solved using an appropriate form of the radiative equilibrium equation (SBLHB), but unfortunately needs a large number of iterations.

## 4 RESULTS AND DISCUSSION

We have calculated a grid of models covering an extensive range of effective temperatures  $2500 \leq T_{eff} \leq 60000$  K and surface gravities  $6 \leq \log g \leq 9$ . In these computations we used 76 depth points to solve the hydrostatic equilibrium and energy transfer equations in the range  $-6 \leq \log \tau \leq 1.5$ .

The continuum radiation field was computed at 87 to 107 frequency points depending on the effective temperature of the model. The points were also chosen taking into account the location of photometric bandpasses used in the colour computations (see Section 4.3).

The temperature-correction procedure was repeated until the temperature changes were everywhere  $\Delta T/T < 0.1\%$ , for most models. In hot models,  $T_{eff} \gtrsim 14000$  K, which are radiative or weakly convective, less than 10 iterations were sufficient to reach the convergence, yielding deviations from flux constancy less than 0.1 per cent everywhere. For lukewarm models,  $9000 \lesssim T_{eff} \lesssim 14000$  K, convergence of  $\Delta F/F < 1\%$  is obtained with about 10 iterations. As the convection becomes more efficient,  $T_{eff} \lesssim 9000$  K, the number of iterations increases to about 40. In the range of temperatures where the onset of the  $H_2$  formation takes place, we need to arise the iteration number to approximately 150, due to the change of the boundary conditions in energy balance equations (see SBLHB).

### 4.1 Atmospheric structure

Strongly convective flux transport develops in the inner layers of cool and lukewarm WD atmospheres. This occurs preferentially in zones where hydrogen is partially ionized or dissociated, which yields a significant drop in the value of the adiabatic temperature gradient favouring the convective instability. Fig. 2 shows the fraction of flux carried by convection in atmospheres with surface gravities  $\log g = 6.5$  and 8.0. It is also shown for  $\log g = 6.5$  models the regions where  $H_2$ , H and  $H^+$  in turn dominate the gas. Convection is absent from the atmosphere in the hotter early stages of a WD. According to our calculations, a superficial convection zone appears as the star cools below  $T_{eff} \approx 12000$  K for WDs with low surface gravities ( $\log g = 6.5$ ) and below  $T_{eff} \approx 16000$  K for more massive stars ( $\log g = 8$ ). The convective zone extends over the region where part of the emergent continuum radiation is formed ( $0.1 \lesssim \tau \lesssim 1$ ).

For cooler models, approximately  $T_{eff} \lesssim 10000$  K for  $\log g = 6.5$  and  $T_{eff} < 11000$  K for  $\log g = 8.0$ , the efficiency of convection increases and a considerable fraction of the flux (more than 90 per cent) is carried by convection in the innermost layers ( $\tau \gtrsim 10$ ). Radiation always dominates in the optically thin layers  $\tau \lesssim 1$ . However, thanks to high densities and molecule formation, a little convective flux persists up to very transparent layers,  $\tau \approx 10^{-3}$ , in atmospheres around  $T_{eff} \approx 4000$  K. The computed models predict a reduction of convection for very cool atmospheres  $T_{eff} \approx 2500$  K, but this result may be affected by non-ideal contributions to the EOS. Slight pressure dissociation of  $H_2$  can be expected at large depths in these models, affecting the profile of the convective flux as consequence of changes in the adiabatic gradient (Saumon & Jacobson 1999).

For  $\log g = 8.0$  models, the convection structure displayed in Fig. 2 is very similar to that showed by Bergeron et al. (1991, Fig. 2) in the common region ( $T_{eff} \geq 5000$  K). As a difference, our results show as the molecular formation (not included in that work) strongly affects this structure below  $T_{eff} = 6000$  K, increasing the convection toward superficial layers.

Results about the run of several physical variables are shown in Figs 3-5 for selected models with different effec-

tive temperatures at  $\log g = 6.5$  and  $8.0$ . For the common models at  $\log g = 8$ , a good agreement is obtained from our  $T(P)$  profiles compared to those by Bergeron, Wesemael & Fontaine (1995a, Fig. 2,  $T_{eff} = 4000 - 10000$  K) and Saumon & Jacobson (1999, Fig. 1,  $T_{eff} = 2500$  and  $3000$  K). The only differences are found in the transparent layers of hot models ( $T_{eff} = 8000 - 10000$  K), where the line blanketing (considered by Bergeron et al.) yields there slight changes in the temperature distribution.

Our sets of models with  $\log g = 6.5$  and  $8.0$  present similar aspects except that higher pressures and densities are found in each model atmosphere with increasing  $g$  (Figs 3-5). In terms of  $T_{eff}$ , it is possible to distinguish roughly three classes of atmospheric structures. One corresponds to hotter models,  $T_{eff} \gtrsim 12000$  K at  $\log g = 6.5$  and  $T_{eff} \gtrsim 14000$  K at  $\log g = 8.0$ , which are purely radiative or with a superficial zone weakly convective. They show rather smooth temperature and density gradients without additional significant details. Throughout these atmospheres, most material is ionized.

As  $T_{eff}$  decreases, a new atmospheric structure takes place. The models with  $T_{eff} \approx 4500-12000$  K at  $\log g = 6.5$  and  $T_{eff} \approx 4500-14000$  K at  $\log g = 8.0$ , cover the range from the onset of convection with little flux transported by it to the models where the molecular formation becomes important. In the present group of models, the relationship between temperature and pressure exhibits (Fig. 3) a clear transition from a very small gradient in radiative outer layers to a steep gradient in the top of the convective zone. In contrast, the run of density with pressure becomes relatively shallow in the transition region between radiative and convective zones (Fig. 5). In this sense, the model  $(T_{eff}, \log g) = (12000, 6.5)$  is interesting, because it shows a slight inversion of the density in approximately  $\log P = 4.7$ . It can be interpreted as result of a too fast temperature rise with increasing  $P$  (see Fig. 3), which is compensated by a decrease of the density ( $P \propto \rho T$ ).

Finally, the coolest models studied,  $2500 \leq T_{eff} \lesssim 4500$  K, show some proper features. They are characterized by molecular formation which, as mentioned earlier, increases the convective efficiency and extends the convective zone toward very transparent regions (Figs 2 and 4), reaching a maximum at  $T_{eff} = 4000$  K. This effect has also been found in very low mass stars with  $\log g = 5$  (SBLHB). At such low  $T_{eff}$ , our models show a uniform temperature in the upper radiative layers and a rather sudden rise with depth in still transparent regions (Fig 4). Deep inside the convective zone results a low temperature gradient, which is very close to the adiabatic value.

Fig. 5 shows that very cool atmospheres extend to extremely high density and pressure regimes (note that the top and bottom layers of all models are located at  $\log \tau = -6$  and  $1.5$ , respectively). Non-ideal effects would actually be very small in models with relatively low gravity  $\log g = 6.5$ , but it can become important in the deep layers (below  $\rho \approx 10^{-2}$ ) of very cool models with  $\log g = 8.0$ . Nevertheless, the  $T(P)$  structures of the atmosphere models are away from the region where Saumon & Chabrier (1992) predict the plasma phase transition of hydrogen (Fig. 3).

Compared to hot and lukewarm models analysed above (except at  $T_{eff}$  around of the onset of convection), the temperature distributions of very cool atmospheres ( $T_{eff} \leq$

$4500$  K) are particularly sensitive to the value of the gravity. The surface temperature decreases and the gradient in the  $(\tau, T)$  plane increases as the gravity is raised (Figs 3 and 4). This is a consequence of the CIA opacity (Section 3.1) which, being a collisional process, becomes stronger in atmospheres with high gravity (therefore more dense) increasing the cooling of upper layers.

## 4.2 Emergent flux distribution

To illustrate the behaviour of the WD spectra in the  $(T_{eff}, g)$  plane, we display in Figs 6a-6f the emergent flux corresponding to some selected  $T_{eff}$  values for  $\log g = 6.5, 8.0$  and  $9.0$ . The importance of different opacity sources can be noted in Fig. 7, where individual contributions to the total monochromatic opacity are shown for some relevant physical conditions. These correspond to a Rosseland optical depth  $\tau = 1$  in atmospheres with  $\log g = 8$  and  $T_{eff} = 60000, 10000, 6000$  and  $2500$  K (from 7a to 7d, respectively). Fig. 7d shows, with heavy lines, the opacity contributions at  $\tau = 0.1$  for the  $2500$  K model.

Emergent fluxes for the three highest values of  $T_{eff}$  clearly show the effect of the atomic hydrogen absorption, which is a dominant source at such high temperatures (Figs 6a-c and 7a-b). Among the spectra present in Fig. 6, only the  $T_{eff} = 60000$  K models show an important radiation flux emerging from the Lyman continuum.

At  $T_{eff} = 15000$  K and  $\log g = 9$ , an important convective zone (with a maximum of 40% of the flux transported by convection) develops between  $\log \tau \approx -1.5$  and  $1.3$ . This strongly affects the Balmer continuum decreasing Lyman and Balmer jumps, with respect to lower gravity models (Fig. 6b). This sensitivity offers the possibility of an observational test of the convection theory even with relatively low-quality data.

Bound-free and free-free process of  $H^-$  and atomic Rayleigh scattering start to take place as the effective temperature diminishes to  $10000$  K. The most prominent feature in the spectra of these atmospheres is the Balmer jump, which markedly weakens for large gravities. We note that these changes in the Balmer jump can also be reproduced by the presence of helium in the atmosphere and an increasing of its abundance (Wegner & Schulz 1981; Bergeron et al. 1991).

A large variety of opacity sources are found in the atmospheres of lukewarm WDs (Fig. 7c), the  $H^-$  opacity being the most important. Since  $H^-$  bound-free opacity is dominant and weakly frequency dependent, the emergent flux of  $T_{eff} = 6000$  K model is relatively featureless and resembles more a blackbody distribution (Fig. 6d). Furthermore, it is relatively insensitive to  $g$ .

Fig. 7d emphasizes the importance of the molecular opacity at  $\tau = 1$  in a  $(T_{eff}, \log g) = (2500, 8.0)$  model. As one proceeds outward in the atmosphere, the opacity becomes completely dominated by CIA process and Rayleigh scattering (heavy lines in Fig. 7d, corresponding to  $\tau = 0.1$ ), due to a marked decrease of the abundance of all species but the  $H_2$  molecule. Besides, as the temperature decreases, separate vibrational bands are clearly identifiable in the CIA opacity. Note that the decrease of the density (from  $\tau = 1$  to  $\tau = 0.1$ ) does not affect the molecular Rayleigh scattering

contribution to the total opacity per gram, because the H<sub>2</sub> remains as the most abundant component.

Synthetic spectra obtained for  $T_{eff} = 2500$  and 4000 K (Figs 6e-f) show a well-known result: the effect of CIA opacity is largest for WDs of low  $T_{eff}$  and high gravity, corresponding to a large abundance of H<sub>2</sub> and high density, and, therefore, a large number density of H<sub>2</sub>-H<sub>2</sub> pairs. The effect of the four vibrational bands of H<sub>2</sub> (Fig. 7d) is clearly visible in the spectrum of models with  $T_{eff} = 2500$  K. This strong absorption over infrared spectral regions coincides with the peak emission of a blackbody at the same  $T_{eff}$ . As a consequence, the stellar flux is forced to emerge at shorter wavelengths, around the minimum in the opacity caused by the H<sub>2</sub> CIA and the Rayleigh scattering.

### 4.3 Colour indices

From the emergent flux provided by the atmospheric model, we can derive magnitudes and colours. We have calculated broadband colour indices using the Johnson-Cousins BVRI and Johnson-Glass JHK response functions of Bessell (1990) and Bessell & Brett (1988), respectively. The magnitude  $m$  corresponding to a bandpass with transmission function  $S_\lambda^m$  was computed from

$$m = -2.5 \log \left[ 4\pi \left( \frac{R}{D} \right)^2 \frac{\int_0^\infty H_\lambda S_\lambda^m d\lambda}{\int_0^\infty S_\lambda^m d\lambda} \right] + c_m \quad , \quad (18)$$

where  $H_\lambda$  is the monochromatic Eddington flux from the model atmosphere for a WD of radius  $R$  and distance  $D$  from Earth. We adopted the calibration constants  $c_m$  given in Bergeron, Ruiz & Leggett (1997, BRL), yielding magnitudes on the Carnegie image tube system. A set of colour indices is obtained from the difference between magnitudes, resulting independent of the radius and distance of the star. Fig. 8 shows the location of the filter transmissions over two illustrative emergent fluxes. We have also calculated the bolometric correction at the visual using the expression derived by Bergeron, Wesemael & Beauchamp (1995b, Eq.[3])

$$BC = 2.5 \log \int_0^\infty H_\lambda S_\lambda^V d\lambda - 10 \log T_{eff} + 15.6165 \quad . \quad (19)$$

In view of increasing attention on very low mass WDs in the last few years, we report the colours and bolometric corrections for a subsample of our grid, corresponding to low gravity ( $\log g = 6.5$ ) and cool ( $T_{eff} = 4000$ -8000 K) models (Table 2). We also show the results for a canonical value  $\log g = 8.0$ .

Fig. 9 shows the ( $V - R, R - I$ ) two-colour diagram for all models calculated. The solid lines connect models with same gravity and  $\log g = 6.5$  (0.5) 9.0 (from top to bottom). Also displayed is a subset of 44 DA stars (filled circles) and 45 non-DA stars (open circles) observed by BRL and having complete BVRI-JHK photometric data <sup>‡</sup>. By comparison, we include the hydrogen atmosphere sequence at  $\log g = 8$  of Bergeron (2000; diamonds), and that of Saumon & Jacobson (1999; triangles) covering  $T_{eff} \leq 4000$  K. The cooling sequence of Richer et al. (2000; dashed line)

<sup>‡</sup> The sample contains WDs from the catalog of McCook & Sion (1987) reclassified DA by BRL.

for a WD with carbon-oxygen core, hydrogen atmosphere and mass  $0.6 M_\odot$  is also shown.

Our models predict that all stars with hydrogen atmospheres above  $T_{eff} \approx 4500$  K, fall on a line of almost constant surface gravity with little dispersion. The DA stars plotted in the figure remain very close to the synthetic colour sequences over the range  $3500 \lesssim T_{eff} \lesssim 8500$  K. In contrast, the non-DA stars reveal more dispersion, although most of them seem to follow the hydrogen sequences. Only a few non-DA stars (marked on the figure) show colour indices strongly affected by other non-hydrogen sources of opacity. Among them, the very low luminosity WD LHS 3250 has a DC classification (continuous spectrum without lines deeper than 5%) and its atmospheric composition is not known (Harris et al. 1999). BPM 27606 is a DQ star (ie. with carbon features) whose spectrum presents very strong C<sub>2</sub> Swan bands (BRL). LP 790 – 29 is also a DQ star.

Fig. 9 shows that the theoretical sequence at  $\log g = 8.0$  of Bergeron (2000) is well reproduced by our models (this occurs also for other  $\log g$  values, not shown here). For the coolest atmospheres ( $T_{eff} < 3500$  K), our sequence at  $\log g = 8$  becomes bluer than that of Saumon & Jacobson (1999). Nevertheless, the three independent models found an equivalent location for the turnoff in  $R - I$ . This turnoff is a consequence of the onset of the H<sub>2</sub> formation (which starts the CIA and molecular Rayleigh opacities), and therefore it varies with the surface gravity. The largest values of  $R - I$  correspond, at instance, to  $T_{eff} = 3500$  K at  $\log g = 6.5$  and  $T_{eff} = 4000$  K at  $\log g = 9.0$ . In agreement with Saumon & Jacobson, we found that several colour indices show the presence of a turnover at low effective temperatures, with  $B - V$  being an exception (see below).

In addition, the cooling curve of Richer et al. (2000) follows the other sequences of models and the sample observed for  $T_{eff} > 4000$  K, but crosses several sequences with different  $g$  for lower  $T_{eff}$  where a constant or smoothly increasing gravity should be expected as the star cools. We also note a certain irregular behaviour where our grid predicts that colours are insensitive to changes in the gravity ( $T_{eff} > 4500$  K).

The ( $B - V, V - K$ ) two-colour diagram is displayed in Fig. 10. There is a close agreement between Bergeron's and our models at  $\log g = 8.0$ , except for the hot models. A similar turnover in  $V - K$  colour (reported earlier by Mould & Liebert 1978) is predicted by both sets of models. Nevertheless, significant departures of our sequence from that of Bergeron can be observed below  $B - V \approx 0.3$  ( $T_{eff} > 7500$  K). These discrepancies presumably have their origin in the hydrogen line opacity and the occupation probability formalism (Hummer & Mihalas 1988) used by his code and not included in our calculations.

The diagram also reveals a certain difficulty of the theory in reproducing the observed values in the  $B - V$  colour at low effective temperatures. In fact, there is an increasing difference between observed and theoretical colour indices above  $B - V \approx 0.7$ . BRL have interpreted this in terms of a pseudo continuum opacity at the Lyman edge (not taken into account in the atmosphere codes), which affects the flux in the  $B$  magnitude (for details see their paper).

Fig. 11 illustrates that the sample of observed stars in the ( $V - I, V - K$ ) diagram is well reproduced by our model grid, which is also in good agreement with the theoretical

**Table 2.** Broadband colour indices of the  $\log g = 6.5$  and  $8.0$  models

$T_{eff}$	$\log g$	$B - V$	$V - R$	$V - K$	$R - I$	$J - H$	$H - K$	BC(V)
4000	6.5	+1.070	+0.689	+2.465	+0.689	+0.226	+0.058	-0.589
4500	6.5	+0.920	+0.594	+2.436	+0.596	+0.403	+0.128	-0.470
5000	6.5	+0.769	+0.499	+2.063	+0.501	+0.362	+0.117	-0.297
5500	6.5	+0.632	+0.418	+1.731	+0.422	+0.324	+0.077	-0.208
6000	6.5	+0.515	+0.351	+1.452	+0.355	+0.287	+0.045	-0.168
6500	6.5	+0.423	+0.298	+1.211	+0.301	+0.248	+0.021	-0.161
7000	6.5	+0.348	+0.254	+0.997	+0.255	+0.207	+0.001	-0.170
7500	6.5	+0.282	+0.216	+0.804	+0.215	+0.169	-0.015	-0.189
8000	6.5	+0.221	+0.180	+0.627	+0.179	+0.133	-0.029	-0.212
4000	8.0	+1.011	+0.653	+1.778	+0.648	-0.029	-0.076	-0.398
4500	8.0	+0.898	+0.581	+2.160	+0.583	+0.271	+0.044	-0.403
5000	8.0	+0.767	+0.499	+2.027	+0.500	+0.341	+0.105	-0.298
5500	8.0	+0.644	+0.423	+1.709	+0.423	+0.300	+0.085	-0.198
6000	8.0	+0.538	+0.360	+1.430	+0.359	+0.261	+0.056	-0.154
6500	8.0	+0.440	+0.305	+1.201	+0.305	+0.232	+0.028	-0.152
7000	8.0	+0.362	+0.260	+1.000	+0.259	+0.200	+0.007	-0.173
7500	8.0	+0.298	+0.223	+0.822	+0.220	+0.169	-0.010	-0.209
8000	8.0	+0.243	+0.192	+0.660	+0.186	+0.136	-0.024	-0.246

sequence of Bergeron. It is also observed that a marked sensitivity of  $V - K$  and  $V - I$  colours to the effective temperature and surface gravity in models beyond the turnover. The reason of this is that  $I$  and  $K$  bandpasses lie just where the  $H_2$  CIA has strong contributions from two major vibrational transitions, while the  $V$  bandpass receives a flux excess that is forced to emerge in the optical spectral range. One would expect that this sensitivity in the WDs with hydrogen atmospheres could be very useful for cosmochronological purposes.

#### 4.4 White dwarfs with low mass

Helium core white dwarf (He WD) stars are considered the final product of the evolution of some close binary systems. The mass of these objects should be smaller than that required for degenerate helium ignition,  $\approx 0.5 M_\odot$  (Mazzitelli 1989), thus, resulting very low mass WDs. They have been detected in large surveys (Bragaglia et al. 1990; Bergeron, Saffer & Liebert 1992; Bragaglia, Renzini & Bergeron 1995; Saffer, Livio & Yungelson 1998), concluding that about 10% of presently known WDs are He WDs.

We have used our atmosphere code to study the changes in colours and absolute visual magnitude of He WDs during the cooling. The calculations were carried out by using the cooling sequences of Benvenuto & Althaus (1998) for helium-core composition and hydrogen envelopes. The chosen evolutionary models cover stellar masses  $M = 0.15, 0.30$  and  $0.45 M_\odot$  with  $M_H/M = 4 \times 10^{-3}, 2 \times 10^{-3}$  and  $4 \times 10^{-4}$ , respectively, where  $M_H$  is the mass of the H envelope. We wish to point out that recent studies (Driebe et al. 1998; Sarna, Antipova & Muslimov 1998; Sarna, Antipova & Ergma 1999) predict the formation of He WDs with massive hydrogen envelopes. Since the H-burning increases with  $M_H$ , thus implying longer evolutionary times, the ages estimated in this paper (using models with rather thin hydrogen envelopes) should be considered as lower limit values.

We summarized here the most important results. Interesting observations can be inferred from the analysis of Fig.

12, which shows evolutionary tracks along with an observational sample of cool stars in  $(J-H, V-K)$  and  $(J-K, R-I)$  two-colour diagrams. The cooling tracks in both diagrams show an almost linear behaviour following the observed photometry up to a predicted effective temperature of approximately 4500 K. Although there is an important scatter of observed colours, it is clear that  $J - H$  and  $J - K$  show a shifting to the blue in the cool extreme of the sample, for DA and non-DA stars. This effect is very well represented by the theoretical cooling sequences, which gets dramatically bluer in these colour indices due to the onset of the  $H_2$  collision-induced absorption for  $T_{eff} \lesssim 4500$  K. Note how the theoretical sequences follow the red edge in  $V - K$  and  $R - I$  of the observational sample, with the less massive models on the right.

Fig. 12 seems to provide observational evidence of the presence of a strong pressure-induced opacity in most of the cool atmospheres. It also suggests that very cool WDs identified as non-DA, could have an important abundance of hydrogen in their atmospheres (perhaps beyond the spectroscopic limit of detection due to the low temperatures). A good example is LHS 1126 (see Fig. 12), the peculiar emergent flux has been interpreted in terms of  $H_2$ -He CIA in a mixed H/He atmosphere with  $\log N(\text{He})/\log N(\text{H}) = 0.8$  (Bergeron et al. 1994).

Another feature exhibited in this figure is the prediction of a second turnover in the  $J - H$  colour (around  $V - K = 0.3$ ) for an advanced stage of the cooling. In this part of the  $(J - H, V - K)$  two-colour diagram, the tracks of stars with different mass coincide, but the cooling times differ significantly. For example, the lowest value of  $J - H$  is reached by a  $0.15 M_\odot$  He WD at 7 Gyr, while a  $0.45 M_\odot$  star needs 16 Gyr more, due to its lower radius and, therefore, to a lower rate of cooling.

In the  $(V - I, M_V)$  colour-absolute magnitude diagram of Fig. 13, the tracks corresponding to masses 0.15, 0.30 and  $0.45 M_\odot$  are shown from right to left. The diagram shows that when a  $0.15 M_\odot$  He WD is older than 5 Gyr, it gets bluer in the  $V - I$  colour. There, the absolute mag-

nitude changes slowly and the star remains brighter than  $M_V = 16.5$  up to 10 Gyr. Similar behaviour is found for more massive models, but a longer time (around 20 Gyr at  $M = 0.45 M_\odot$ ) is spent by these stars before the turnover in  $V - I$  takes place, as a consequence of an abundant  $H_2$  formation in their atmospheres.

A number of observed WDs appear redward in  $V - I$  of the  $0.45 M_\odot$  sequence. Since the stellar evolution theory predicts that single WDs with very low mass cannot be formed within the lifetime of the Galaxy, those stars in the diagram correspond to unresolved (or barely resolved) double degenerate systems which appear overluminous, or single low mass WDs forming a binary system with a much less luminous companion.

We have used our code to derive atmospheric parameters, effective temperature and surface gravity, for five of these stars using photometric data of BRL. Combining these with evolutionary results we have also derived masses and ages for the stars. The effective temperature can be constrained from atmosphere fits to the observed colour indices. However, the surface gravity is poorly determined by this procedure for hot stars ( $T_{eff} \gtrsim 4500$  K), because the colours are rather insensitive to changes of  $g$  in such models. Nevertheless, it is possible to derive the gravity and the mass of a star when its absolute magnitude is known. Therefore, we determine the effective temperature, the surface gravity and the mass of each star, fitting simultaneously its absolute visual magnitude and colours with a least-squares method. The  $B - V$  colour was not included in this procedure because there is an opacity source affecting the  $B$  filter, which is not considered in the model (see Section 4.3). The mass-radius relations employed in the fitting and the evolution ages were taken from models kindly provided by Benvenuto & Althaus (2000, private communication). All interior models used here have hydrogen envelopes.

Treating the observed objects as single WDs, we obtain the results summarized in Table 3. Successive columns give the WD identifier, name, effective temperature, surface gravity, estimated mass, mean deviation of the magnitude and colour fitting, calculated and observed absolute visual magnitude, and age. The quoted errors have been determined as the changes necessary to produce a mean uncertainty of  $2\sigma$  provided by the fitting procedure.

The effective temperatures determined here are on average 65 K hotter than those previously estimated by BRL. These differences are not significant against to the mean errors of both calibrations (120 K here and 110 K in the BRL work). As discussed above, the determination of the  $T_{eff}$  is mainly provided by the broad-band fit, whereas the temperature uncertainties can be significantly constrained by the absolute magnitude fit.

Our  $\log g$  values are 0.1 larger than the results of BRL, and we also obtain systematically larger mass for these stars (by  $\approx 0.06 M_\odot$ ), in part due to the use of different mass-radius relations. Furthermore, using the helium core models of Benvenuto & Althaus, we estimated ages about twice than the BRL determinations, who used carbon core models of Wood<sup>§</sup>. These differences have an origin mainly in that

the heat content stored per gram in a helium core is larger than that of carbon (or carbon-oxygen) core for fixed temperature. Consequently, He WDs remain bright for comparatively longer times, while the C and C-O WDs cool more rapidly.

Among the five stars analysed here, only L870-2 is confirmed as binary. This star is a double-lined spectroscopic binary composed of a detached pair of DA WDs (Saffer, Liebert & Olszewski 1988). LHS 239 is a component of a resolved binary (e.g. Poveda, Herrera, Allen, Cordero & Lavalley 1994). Its companion is LHS 240, a WD classified DC9 in the McCook & Sion catalog (1987). For LHS 239, BRL have found a discrepancy between the effective temperature derived from its energy distribution (colour-fit) and that obtained from spectroscopy (fit to  $H\alpha$  line profile). They consider that it could be explained if this object is itself an unresolved double system. The remain stars in the sample (G141-2, G187-8 and G128-7) are suspected double degenerate binary (BRL) because their derived masses fall below  $0.4 M_\odot$  and the current theories attribute to such WDs a binary origin.

Table 4 shows the results of interpreting this group of stars as unresolved binaries containing two identical WDs. The combined mass estimated for these systems is below the Chandrasekhar limit, although the individual stars are too massive to have helium cores, except perhaps in the case of L870-2. It is worth noting that combinations of two different atmospheres (not analysed here) could allow mixed systems of He WD + CO WD. The effective temperatures in Table 4 are equivalent to those deduced from a single WD fitting due to the lack of sensitivity to gravity variations of colours, except for LHS 239.

From a detailed spectroscopic analysis Bergeron, Wesemael, Liebert & Fontaine (1989) have deduced that L870-2 is composed of a pair of DA WDs with comparable effective temperatures ( $T_1 = 7470$  K and  $T_2 = 6920$  K) and masses ( $M_1 = 0.47 M_\odot$  and  $M_2 = 0.52 M_\odot$ ). For these determinations, they adopted the zero-temperature mass-radius relation of Hamada-Salpeter (1961). Assuming identical components for the system and using both helium core and carbon-oxygen core models recently available, we confirm that their individual masses are within the core-helium ignition limit ( $\approx 0.45 - 0.50 M_\odot$ , see Table 4). Our result for the effective temperature ( $T_{eff} = 7200$  K) is intermediate between those deduced by Bergeron et al..

We note that LHS 239 cannot be modelled satisfactorily by a binary with identical components (the mean deviation of the fit,  $\sigma = 0.13$ , is much larger than the uncertainty of the observed magnitude,  $\sigma_{obs} = 0.03$ ), while a good fit is obtained considering this star as a single object ( $\sigma = 0.05$ ). These results suggest that the photometry observed for LHS 239 corresponds to a single He-core WD. We consider that another origin, different to unresolved binary possibility, would be need to explain the discrepancy in the calibrations of  $T_{eff}$  obtained by BRL (see above).

The photometric fits for G141-2 and G187-8 do not show any clear preference between the single WD or unresolved binary interpretations. In particular, we have not found a very satisfactory hydrogen atmosphere fit to the observed colour indices for these stars, perhaps due to a significant presence of helium or metals in their atmospheres. For G128-7, a good fit is obtained for both single and dou-

<sup>§</sup> Evolutionary models of helium core WDs are available only recently.

**Table 3.** Fundamental parameters of low mass white dwarfs assuming a single helium core star

WD	Name	$T_{eff}$ (K)	$\log g$	$M/M_{\odot}$	$\sigma$ (mag)	$M_{V\ cal}$	$M_{V\ obs}$	Age (Gyr)
0135 – 052	L870 – 2	7200±80	7.28±0.08	0.30±0.02	0.03	12.41	12.40±0.07	1.8±0.3
0747 + 073A	LHS 239	4210±50	7.71±0.08	0.44±0.04	0.05	15.65	15.65±0.03	11.8±1.5
1818 + 126	G 141 – 2	6450±200	7.40±0.11	0.33±0.03	0.10	13.06	13.04±0.50	2.2±0.1
2048 + 263	G 187 – 8	5250±150	7.46±0.15	0.34±0.06	0.12	14.14	14.12±0.15	4.0±1.3
2248 + 293	G 128 – 7	5600±80	7.55±0.07	0.37±0.03	0.05	13.94	13.94±0.19	3.3±0.2

**Table 4.** Parameters derived assuming a binary with two identical degenerate stars

WD	core	$T_{eff}$ (K)	$\log g$	$M/M_{\odot}$	$\sigma$ (mag)	$M_V$ (binary)	Age (Gyr)
0135 – 052	He	7200±80	7.81±0.05	0.50±0.02	0.03	12.41	2.5±0.2
	CO	7200±80	7.78±0.04	0.47±0.02	0.03	12.40	1.1±0.1
0747 + 073A	CO	4180±70	8.22±0.16	0.72±0.10	0.13	15.65	8.6±1.0
1818 + 126	CO	6450±200	7.92±0.10	0.54±0.06	0.09	13.04	1.7±0.4
2048 + 263	CO	5250±170	7.98±0.15	0.57±0.09	0.12	14.12	3.8±1.1
2248 + 293	CO	5600±80	8.09±0.06	0.64±0.04	0.05	13.94	3.5±0.2

ble star possibilities. Unfortunately, for the deduced effective temperature (5600 K), the energy distribution is gravity-insensitive and the fits do not highlight the binary nature of this star. Additional spectroscopic data and line calculations could improve the energy distribution fits and the identification of the components of these and other (suspected) unresolved binaries.

## 5 CONCLUSIONS

We have computed a grid of hydrogen model atmospheres for white dwarfs covering an extensive region in the ( $T_{eff}, g$ ) plane. For this, we have employed a partial method of linearization of equations for stellar atmospheres in which the energy is transported by radiation and convection. In view of numerical instabilities usually found to solve the resulting set of equations, we use a suitable initial temperature distribution which improves the convergence properties taking into account the low values of temperature gradient expected in deep layers of convective models.

From a relatively simple thermodynamic model, we have derived analytical expressions for the adiabatic temperature gradient and heat capacities of a mixture of hydrogen species. They result appropriate and easy to apply in the calculation of the convective flux. In particular, for the density regimes present in most of the atmospheres studied, our expression of the adiabatic gradient successfully reproduces the values of the ideal equation of state developed by Saumon & Chabrier.

We have analysed in detail the structure and emergent flux of hydrogen white dwarf atmospheres over a wide range of effective temperatures and gravities. This analysis complements the most recent studies, to provide an overall picture of these atmospheres and the changes to them expected during the cooling. In particular, we find strong modifications of the emergent flux for  $T_{eff} \lesssim 4500$  K produced by the pressure-induced absorption of molecular hydrogen. The results obtained from our code have been compared to those recently published. Our calculations confirm the importance of infrared photometry for the study of cool white dwarfs,

and its use in the determination of ages of the Galaxy and globular clusters.

Spectral evolution of helium core white dwarfs has briefly been studied using evolutionary sequences recently available for these objects. Colour-colour diagrams show that the theoretical cooling sequences follow the low mass boundary at the cool extreme of an observational sample of white dwarfs. It is very interesting to note that on a timescale less than 9 Gyr, very low mass He WDs (0.15  $M_{\odot}$ ) show strongly non-blackbody colours with absolute visual magnitude that are still below 16.5, while massive He WDs ( $\approx 0.45 M_{\odot}$ ) remains brighter than  $M_V = 17$  for 25 Gyr.

Combining atmosphere calculations with interior model results, we determined the possible fundamental parameters of some low mass white dwarfs. Because, in general, very low mass WDs are suspected to be close binaries, the estimated parameters depend on the possible components of each system. With the assumption that both components are identical, the analysed stars present preferentially carbon-oxygen core compositions but with combined masses below the Chandrasekhar limit.

We will present self-consistent cooling calculations in the near future, by incorporating our atmosphere code as an appropriate surface boundary condition for evolutionary models of white dwarfs.

### Acknowledgments

I am deeply grateful to O. Benvenuto and L. Althaus for encouraging me to perform this study. I thank them for many useful and stimulating discussions, and their thorough reading of the manuscript. L. Althaus has provided me with invaluable help for this investigation. His suggestions and contributions resulted in substantial improvements to the atmosphere code and the results presented here. I am also grateful to D. Saumon, who offered significant comments and provided me with his abundance and colour calculations for comparison. It is a pleasure to thank P. Bergeron for kindly making available his colour calculations and A. Borysow for providing the updated cross-sections for the collision-induced absorption by H<sub>2</sub>. Many thanks are due to N. Cepeda and M. Gomez for kindly revising the English

text. I wish to thank also the referee for his useful remarks which improved the earlier version of this paper.

## REFERENCES

- Alcock C. et al., 1997, ApJ, 491, L11  
 Alcock C. et al., 1999, ApJ, 518, 44  
 Althaus L. G., Benvenuto O. G., 2000, MNRAS 317, 95  
 Auer L., Mihalas D., 1970, MNRAS 149, 60  
 Avrett E., Krook M., 1963, ApJ, 137, 874  
 Bell K. L., Berrington K. A., 1987, J. Phys. B, 20, 801  
 Benvenuto O. G., Althaus L. G., 1998, MNRAS, 293, 177  
 Bergeron P., 2000, private communication  
 Bergeron P., Wesemael F., Liebert J., Fontaine G., 1989, ApJ, 345, L91  
 Bergeron P., Wesemael F., Fontaine G., 1991, ApJ, 367, 253  
 Bergeron P., Saffer R. A., Liebert J., 1992, ApJ, 394, 228  
 Bergeron P., Wesemael F., Fontaine G., 1992, ApJ, 397, 288  
 Bergeron P., Ruiz M. T., Leggett S. K., Saumon D., Wesemael F., 1994, ApJ, 423, 456  
 Bergeron P., Saumon D., Wesemael F., 1995a, ApJ, 443, 764  
 Bergeron P., Wesemael F., Beauchamp A., 1995b, PASP, 107, 1047  
 Bergeron P., Ruiz M. T., Leggett S. K., 1997, ApJS, 108, 339 (BRL)  
 Bessell M. S., 1990, PASP, 102, 1181  
 Bessell M. S., Brett J. M., 1988, PASP, 100, 1134  
 Borysow A., Jorgensen U. G., Zheng C., 1997, A&A, 324, 185  
 Bragaglia A., Greggio L., Renzini A., D'Odorico S., 1990, ApJ, 365, L13  
 Bragaglia A., Renzini A., Bergeron P., 1995, ApJ, 443, 735  
 Chabrier G., 1999, ApJ, 513, L103  
 Cox J. P., Giuli R. T., 1968, Principles of Stellar Structure, New York: Gordon and Breach  
 D'Antona F., Mazzitelli I., 1979, A&A, 74, 161  
 D'Antona F., Mazzitelli I., 1990, ARA&A, 28, 139  
 Dalgarno A., Williams D., 1966, Proc. Phys. Soc. G.B., 85, 685  
 Driebe T., Schonberner D., Blocker T., Herwig F., 1998, A&A, 339, 123  
 Edmonds P. D., Grindlay J., Cool A., Cohn H., Lugger P., Bailyn C., 1999, ApJ, 516, 250  
 Fontaine G., Graboske H. C. Jr., Van Horn H. M., 1977, ApJS, 35, 293  
 Fontaine G., Michaud G., 1979, ApJ, 231, 826  
 Fontaine G., Villeneuve B., Wilson J., 1981, ApJ, 243, 550  
 Graboske H. C. Jr., Harwood D. J., Rogers F.J., 1969, Phys. Rev., 186, 210  
 Gray D.F., 1992, The observation and analysis of stellar atmospheres, 2d ed., Cambridge Univ. Press, p. 136  
 Grenfell T. C., 1974, A&A, 31, 303  
 Gustafsson B., 1971, A&A, 10, 187  
 Gustafsson B., Nissen P. E., 1972, A&A, 19, 261  
 Hamada T., Salpeter E.E., 1961, ApJ, 134, 683  
 Hansen B. M. S., 1998, Nature, 394, 860  
 Hansen B. M. S., 1999, ApJ, 520, 680  
 Hare W. F. J., Welsh H. L., 1958, Can. J. Phys., 36, 88  
 Harris H. C., Dahn C. C., Vrba F. J., Henden A. A., Liebert J., Schmidt G. D., Reid I. N., 1999, ApJ 524, 1000  
 Hummer D. G., Mihalas D., 1988, ApJ, 331, 794  
 Iben I. Jr., Tutukov A. N., 1984, ApJ, 282, 615  
 Iben I. Jr., MacDonald J., 1985, ApJ, 296, 540  
 Irwin A. W., 1981, ApJS, 45, 621  
 John T., 1988, A&A, 193, 189  
 Koester D., 1976, A&A, 52, 415  
 Koester D., 1980, A&ASS, 39, 401  
 Krishna-Swamy K.S., 1961, ApJ, 134, 1017  
 Kurucz R., 1970, Smithsonian Obs. Spec. Rep., 308  
 Lenzuni P., Chernoff D.F., Salpeter E.E., 1991, ApJS, 76, 759  
 Lenzuni P., Saumon D., 1992, RMxAA 23, 223  
 Marsh T. R., 1995, MNRAS, 275, L1  
 Mazzitelli I., 1989, ApJ, 340, 249  
 McCook G.P., Sion E.M., 1987, ApJS, 65, 603  
 Menzel D.H., Pekeris C.L., 1935, MNRAS, 96, 77  
 Mihalas D., 1965, ApJ, 151, 564  
 Mihalas D., 1978, Stellar Atmospheres, 2d ed., San Francisco: Freeman  
 Monet D., Dahn C. C., Vrba F. J., Harris H. C., Pier J. R., Luginbuhl C. B., Ables H. D., 1992, AJ, 103, 638  
 Moran C., Marsh T. R., Bragaglia A., 1997, MNRAS, 288, 538  
 Mould J., & Liebert J., 1978, ApJ, 226, L29  
 Muchmore D., 1984, ApJ, 278, 769  
 Neale L., Tennyson J., 1995, ApJ, 454, L169  
 Nordlund A., 1974, A&A, 32, 407  
 Poveda A., Herrera M. A., Allen C., Cordero G., Lavalley C., 1994, RMxAA 28, 43  
 Renault C. et al., 1997, A&A 324, L69  
 Richer H. B., Hansen B., Limongi M., Chieffi A., Straniero O., Fahlman G. G., 2000, ApJ 529, 319  
 Saffer R. A., Liebert J., Olszewski E. M., 1988, ApJ, 334, 947  
 Saffer R. A., Livio M., Yungelson L. R., 1998, ApJ, 502, 394  
 Sarna M. J., Antipova J., Ergma E., 1999, 11th. European Workshop on White Dwarfs (Solheim J.-E., Meistas E.G., Eds.) ASP Conference Series, 169, 400  
 Sarna M. J., Antipova J., Muslinov A., 1998, ApJ, 499, 407  
 Saumon D., 1999, private communication  
 Saumon D., Bergeron P., Lunine J.I., Hubbard W.B., Burrows A., 1994, ApJ, 424, 333 (SBLHB)  
 Saumon D., Chabrier G., 1992, Phys. Rev. A, 46, 2084  
 Saumon D., Chabrier G., Van Horn H. M., 1995, ApJS, 99, 713, (SCVH)  
 Saumon D., Jacobson S. B., 1999, ApJ, 511, L107  
 Sauval A. J., Tatum J. B., 1984, ApJS, 56, 193  
 Van Kerwijk M. H., Bergeron P., Kulkarni S. R., 1996, ApJ, 467, L89  
 Vauclair G., Reisse C., 1977, A&A, 61, 415  
 von Hippel T., Gilmore G., Jones D. H. P., 1995, MNRAS, 273, L39  
 von Hippel T., Gilmore G., 2000, AJ 120, 1384  
 Wegner G., Schulz H., 1981, A&AS, 43, 473  
 Wesemael F., Bergeron P., Fontaine G., Lamontagne R., 1991, in 7th European Workshop on White Dwarfs, ed. G. Vauclair & E. M. Sion (NATO ASI Series) (Dordrech: Kluwer), 159  
 Winget D. E., Hansen C. J., Liebert J., Van Horn H. M., Fontaine G., Nather R. E., Kepler S. O., Lamb D. Q., 1987, ApJ 315, L77  
 Wood M. A., 1992, ApJ, 386, 539
- **Figure 1.-** Comparisons of values for the adiabatic temperature gradient  $\nabla_A = \partial \ln T / \partial \ln P|_S$ , obtained from SCVH EOS (dotted lines) and our expression (Eqs. (5-7), solid lines) calculated for different atmosphere models at  $\log g = 8$  (with effective temperatures indicated on the plot).
  - **Figure 2.-** The structure of the convection zones for models with  $\log g = 6.5$  and  $8.0$ . Curves show the layers where convection carries 1, 10 (20) 90 and 95 per cent (from bottom to top) of the total flux at  $\log g = 6.5$  (solid lines) and  $8.0$  (dashed lines). The dotted curves show from left to right 95, 50 and 5% of  $H_2$  abundance, and 5, 50 and 95% of  $H^+$  abundance for models at  $\log g = 6.5$ .
  - **Figure 3.-** Temperature-pressure stratifications for atmosphere models with  $\log g = 6.5$  (solid lines) and  $8.0$  (dotted lines). Models shown have  $T_{eff} = 2500$  (250) 4000, 4500, 5000 (1000) 12000, 15000 (5000) 30000 (10000) 60000 K (from bottom to top). For models at  $\log g = 6.5$ , the tri-

angles indicate the  $\tau = 2/3$  level, and the circles show the regions where convection carries 1% of the total flux near the transition between radiative and convective zones. The plasma phase transition predicted by Saumon & Chabrier (1992) is represented by the heavy curve labeled ‘‘PPT’’. This figure extends the results in Fig. 2 of Bergeron et al. (1995a).

- **Figure 4.-** Runs of temperature with Rosseland mean optical depth for models presented in Fig. 3. Solid circles indicate the top of the convective zone of models at  $\log g = 6.5$ .

- **Figure 5.-** Density profiles for models as those referred to in Fig. 4. Visible extremes of each curve are located at  $\log \tau = -6$  (bottom) and 1.5 (top).

- **Figure 6.-** Emergent flux distributions for various effective temperatures (indicated on the plot) and  $\log g = 6.5$  (solid lines), 8.0 (dashed lines) and 9.0 (dash-dotted lines). Those are compared with a blackbody spectrum at the same  $T_{eff}$  (dotted lines).

- **Figure 7.-** In an obvious notation, individual contributions to the opacity at a depth  $\tau = 1$  of the models with  $\log g = 8.0$  and  $T_{eff} = 60000, 10000, 6000$  and 2500 K, from (a) to (d). These correspond to  $(\log T, \log \rho) = (4.76, -6.53), (4.03, -5.75), (3.80, -4.15), (3.53, -1.13)$ , respectively. Heavy lines in (d) indicate the most important opacity contributions at  $\tau = 0.1$  of the 2500 K model, where  $(\log T, \log \rho) = (3.09, -2.46)$ .

- **Figure 8.-** Normalized profiles of emergent fluxes for  $T_{eff} = 2500$  (dashed line) and 10000 K (solid line) at  $\log g = 8$ , and the blackbody profile at 2500 K (dash-dotted line). Dots indicate the filter transmissions of *BVRI* Johnson-Cousins and *JHK* Johnson-Glass systems.

- **Figure 9.-** The  $(V - R, R - I)$  two-colour diagram shows hydrogen model atmospheres of white dwarfs. Heavy solid lines represent our models at  $\log g = 6.5$  (0.5) 9.0 from top to bottom, while thin lines connect those with the same  $T_{eff}$  (labeled). It is also shown the  $\log g = 8.0$  sequences of Saumon & Jacobson (1999; triangles) and Bergeron (2000; diamonds); and the cooling track for a  $0.6-M_{\odot}$  carbon-oxygen WD calculated by Richer et al. (1999; dashed line). Photometric data of DA (filled circles) and non-DA (open circles) stars are taken from BRL, except the colour indices of LHS 3250 which are taken from Harris et al. (1999).

- **Figure 10.-** The  $(B - V, V - K)$  colour-colour diagram shows the photometric data of BRL (circles), the  $\log g = 8.0$  sequence of Bergeron (diamonds) and our model grid (lines). Notation is as Fig. 9.

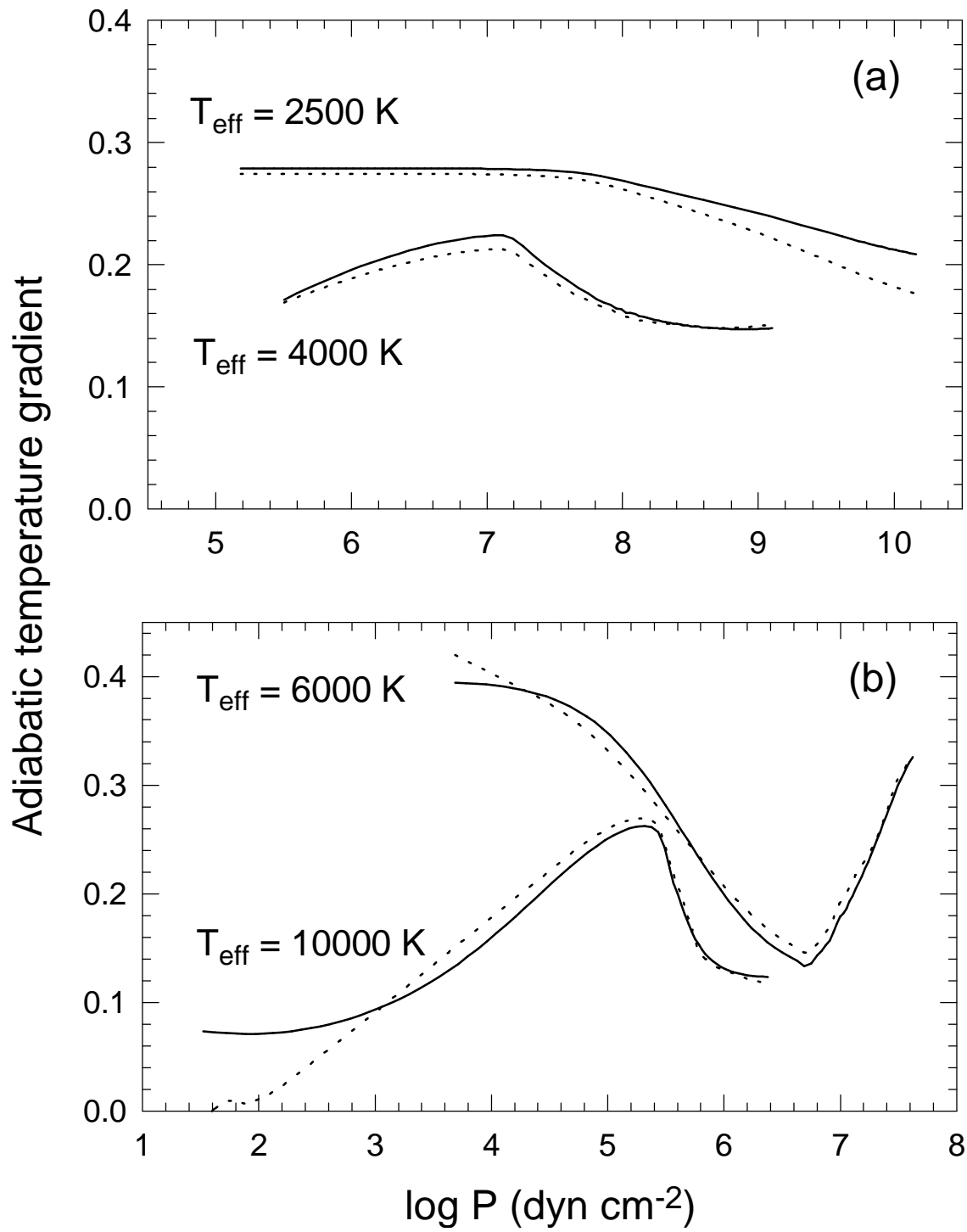
- **Figure 11.-** Same as Fig. 10 for the  $(V - I, V - K)$  diagram.

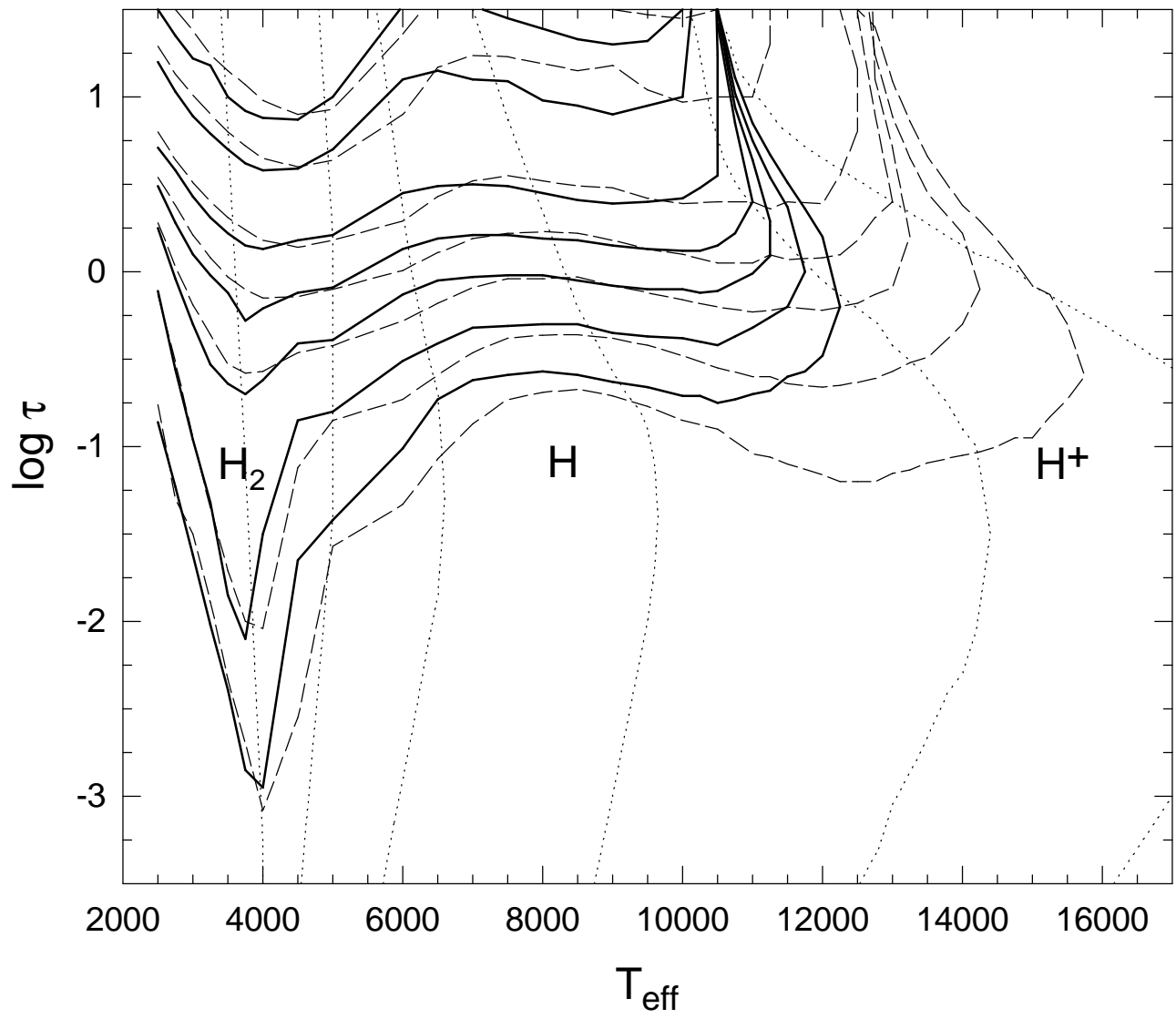
- **Figure 12.-** Evolutionary tracks of He WDs with masses 0.15, 0.30 and  $0.45 M_{\odot}$  (solid lines from right to left) displayed in  $(J - H, V - K)$  and  $(J - K, R - I)$  two-colour diagrams. A subset of cool WDs observed by BRL is represented with filled (DA) and open circles (non-DA WDs). Ages in Gyr are labeled for 0.15 and  $0.45-M_{\odot}$  models. Dashed lines indicate the cooling track of a black body (independently of its size!).

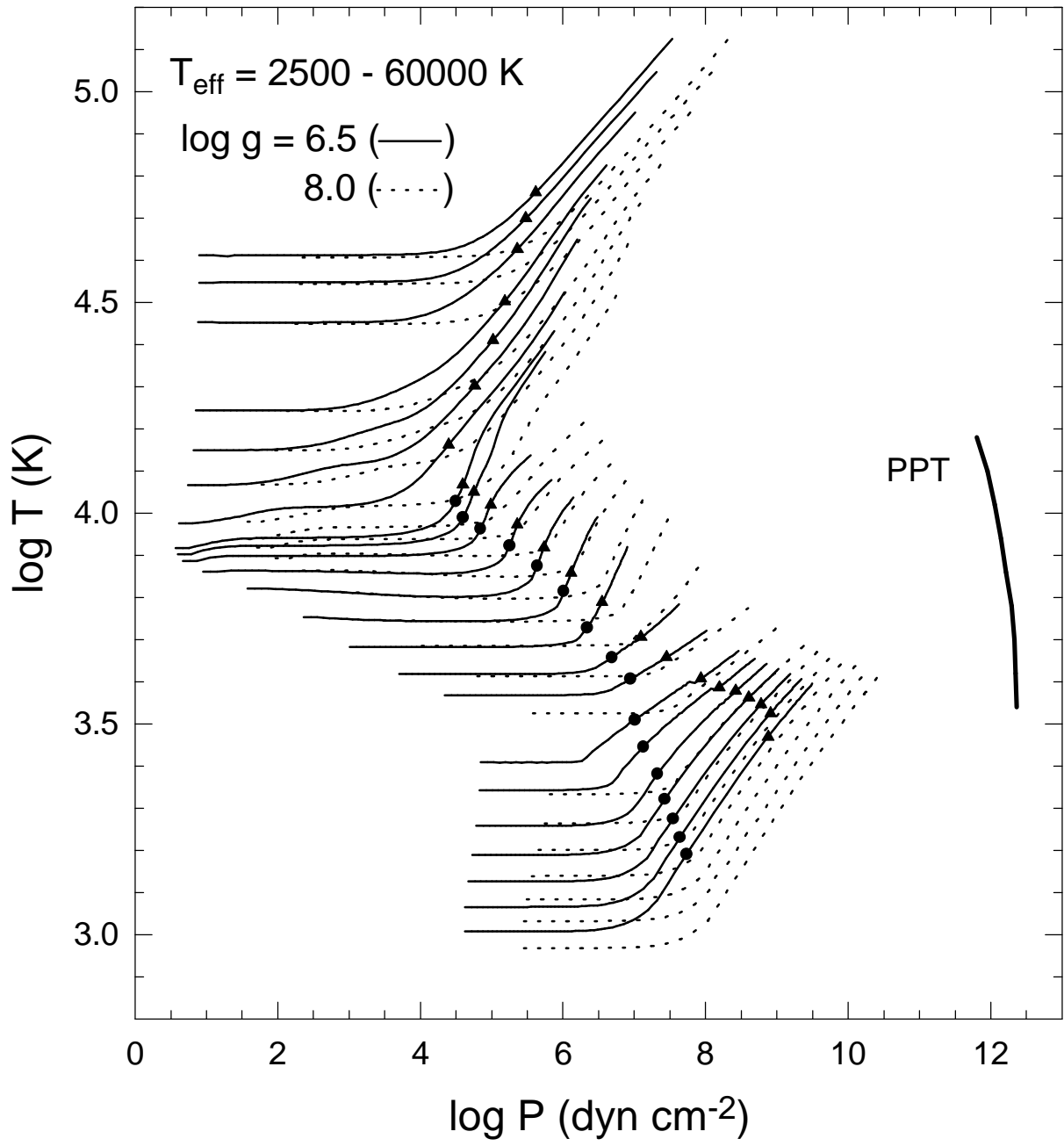
- **Figure 13.-** The colour-absolute magnitude diagram shows the cooling tracks of WDs with helium cores, hydrogen atmospheres and masses 0.15, 0.30 and  $0.45 M_{\odot}$  (solid lines from right to left). Ages are indicated in units of  $10^9$

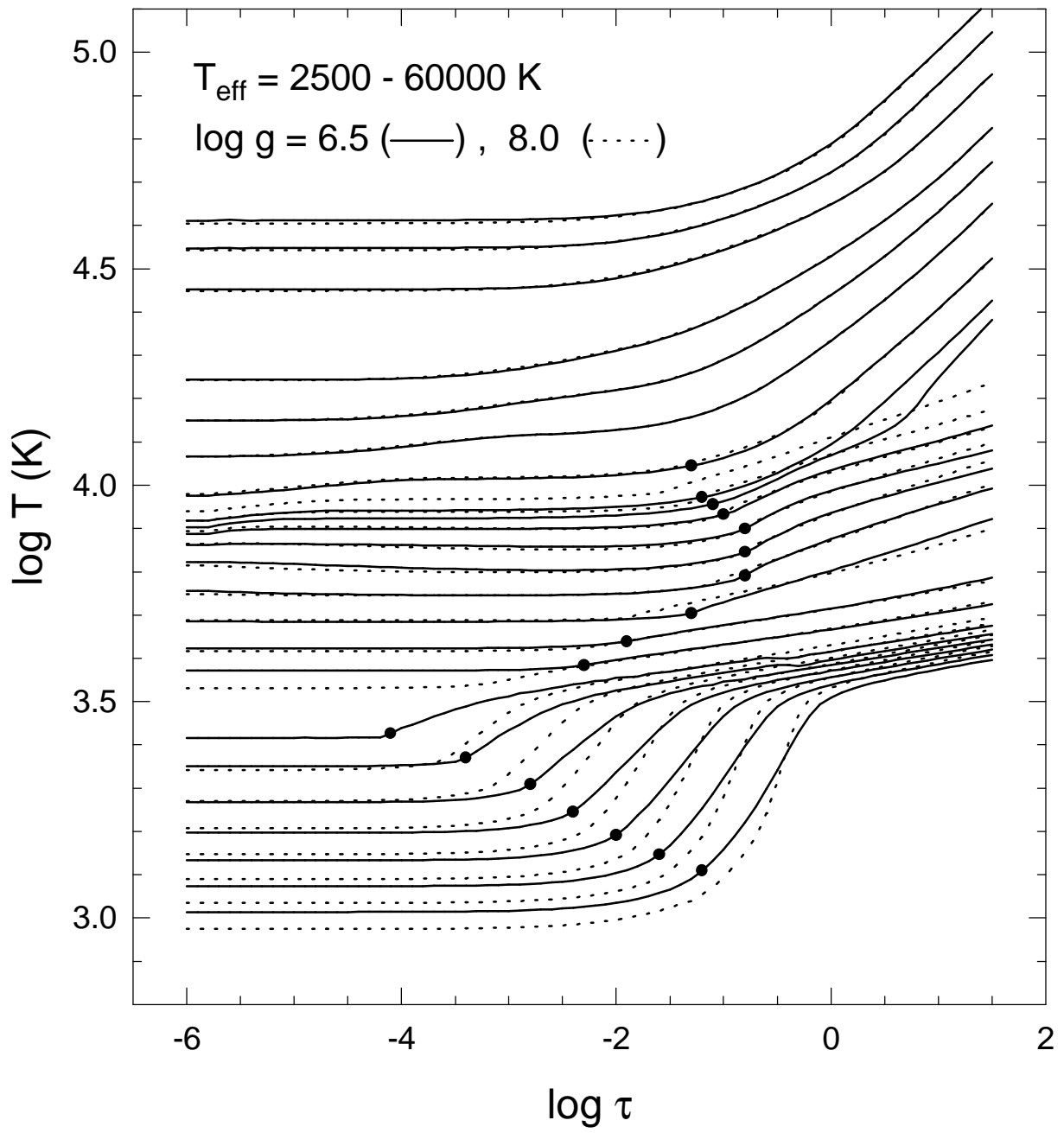
years. Dotted lines show the same cooling tracks assuming stellar radiation as black body. The observed photometry is taken from BRL (DA WDs: filled circles; non-DA WDs: open circles); Monet et al. (1992; diamonds) and Harris et al. (1999; LHS 3250).

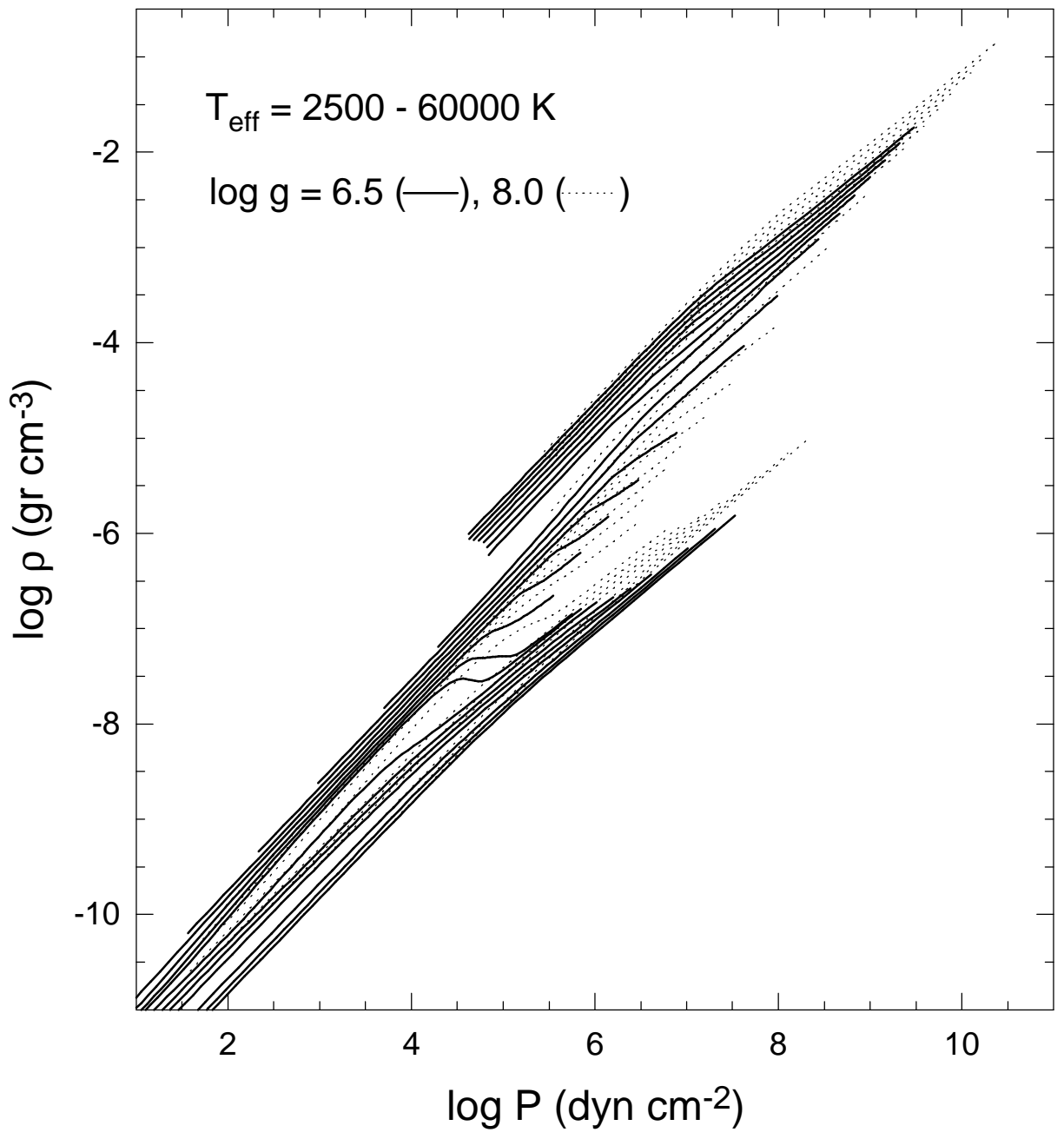
This paper has been produced using the Royal Astronomical Society/Blackwell Science L<sup>A</sup>T<sub>E</sub>X style file.

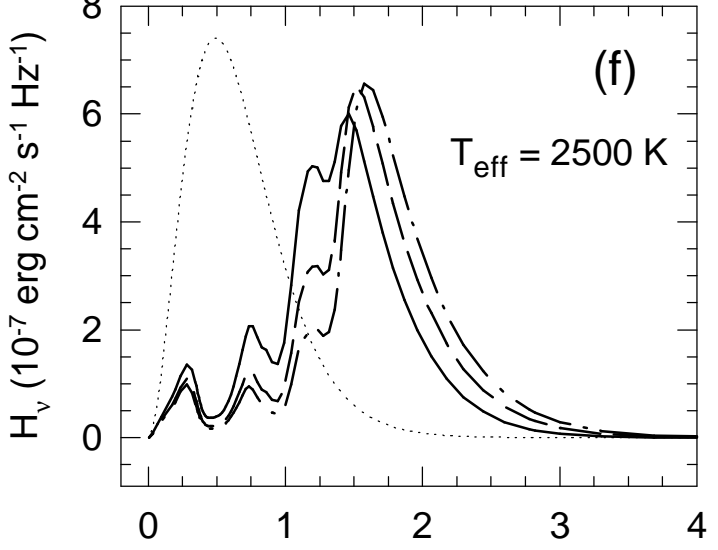
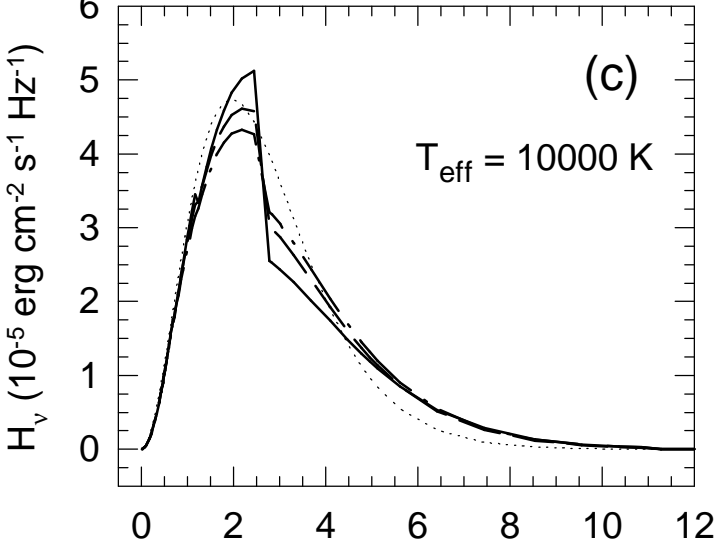
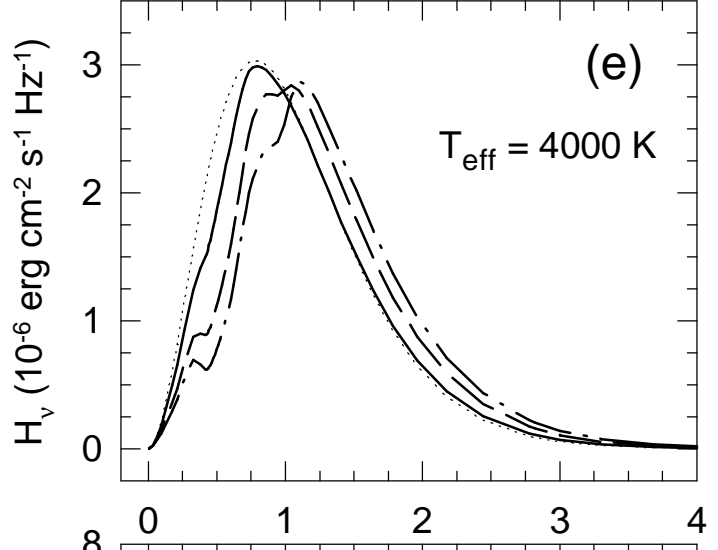
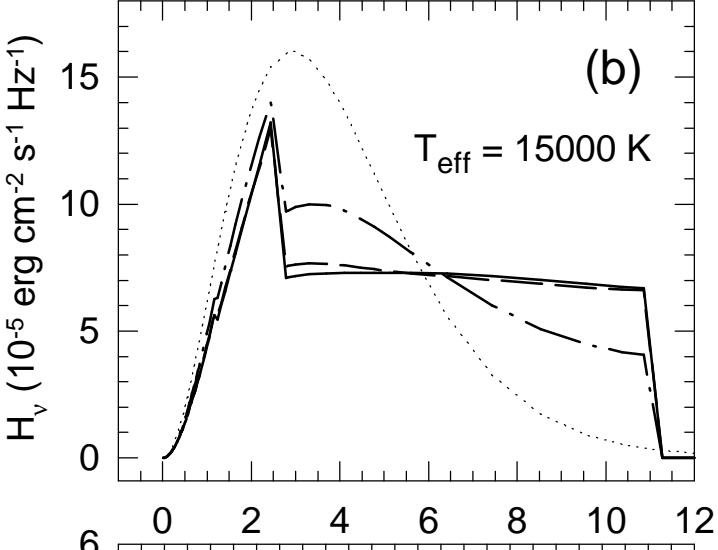
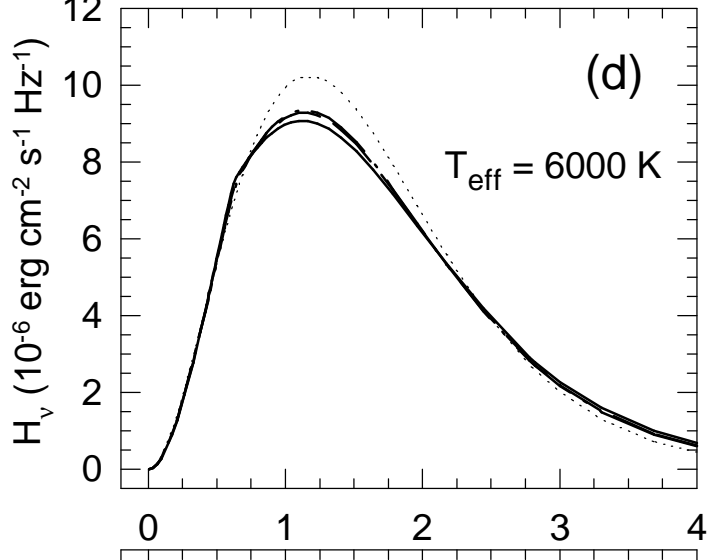
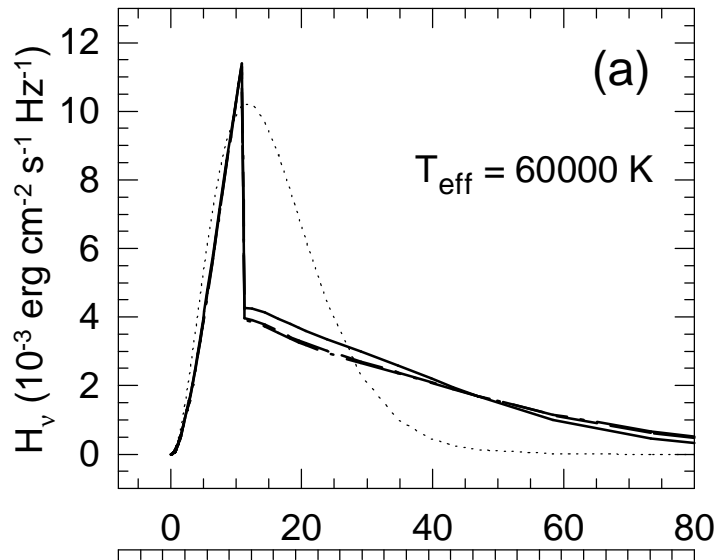












Frequency ( $\mu\text{m}^{-1}$ )

